Thermal boundary resistance and diffusivity measurements on thin $YBa_2Cu_3O_{7-x}$ films with MgO and $SrTiO_3$ substrates using the transient grating method

C. D. Marshall and A. Tokmakoff
Department of Chemistry, Stanford University, Stanford, California 94305

I. M. Fishman
Hansen Experimental Physics Laboratory, Stanford University, Stanford, California 94305

C. B. Eom and Julia M. Phillips
AT&T Laboratories, Murray Hill, New Jersey 07974

M. D. Fayer
Department of Chemistry, Stanford University, Stanford, California 94305

(Received 20 July 1992; accepted for publication 30 September 1992)

Interface selective transient grating experiments are performed on oriented thin films ($\sim$100 nm) of $YBa_2Cu_3O_{7-x}$, with MgO and $SrTiO_3$ substrates. The anisotropic $YBa_2Cu_3O_{7-x}$ thermal diffusivity constants and the thermal boundary resistance between the thin film and substrate are measured. Four different excitation and probe geometries are utilized such that each geometry results in a unique temporal decay. The grating has a significant amplitude on both sides of the film–substrate interface with a grating wave vector parallel to the interface. The four experimental geometries comprise an over-determined system that can be used to confirm the validity of the model assumptions. Numerical fits to the experimental data, using a straightforward diffusive model, are performed to obtain information on thermal diffusivity and to demonstrate the applicability of the technique to monitor anisotropic thermal relaxation processes in thin film–substrate structures.

I. INTRODUCTION

Thermal boundary resistance measurements on high temperature superconducting thin films have attracted considerable attention over the past several years.[1–6] Much of the interest has arisen from device applications such as infrared detectors based on the bolometric effect.[7,8] A detailed understanding of the thermal contact between the film and its supporting substrate is required for this application. At the relatively elevated temperatures ($>$77 K) typically utilized for high temperature superconductors, the low temperature acoustic mismatch model predicts a boundary resistance (Kapitza temperature jump) that is $\sim$10–100 times smaller than has been measured experimentally between $YBa_2Cu_3O_{7-x}$ (YBCO) films and a variety of substrates.[1–6]

In a recent article[5] the transient grating method (see Fig. 1) was applied to measure the thermal diffusivity constants and boundary resistance in thin films of YBCO on MgO crystalline substrates. A combination of excitation and probe diffraction geometries was used[9] to extract the thermal parameters. In modeling the results the substrate was assumed to have infinite thermal conductivity, i.e., the substrate acted as a perfect heat sink. That was a reasonable approximation since MgO has $\sim$50 times larger thermal conductivity than YBCO in the direction of the surface normal. The measurements reported in this paper extend on our previous transient grating studies to include the effects of finite thermal conductivity inside $SrTiO_3$ and MgO substrates. The more detailed analysis presented in this paper was necessary because the $SrTiO_3$ substrate has a much smaller ($\sim$5 times) thermal conductivity than MgO, which in turn leads to a significant breakdown of the perfect heat sink approximation. For finite thermal conductivity of the substrate, the thermal grating extends to both sides of the interface. A theory that includes diffraction from such transient gratings has been recently developed.[10] The focus of this paper is the detailed application of this theory to study thermal flow in YBCO thin films in epitaxial contact with $SrTiO_3$ and MgO substrates. The quality of fits for the YBCO–MgO system is significantly improved over our previous work.[5] This is due to more complete description used to model both the thermal flow and the diffraction efficiency from both sides of the interface. Anisotropic bulk thermal diffusivity constants in thin films of YBCO are measured and the thermal boundary resistance is determined.

II. EXPERIMENTAL PROCEDURES

The output of a Q-switched, mode-locked Nd:YAG laser is frequency-doubled to a wavelength of 532 nm and used to excite a sync-pumped dye laser operating at a wavelength of 561 nm. The dye laser is cavity dumped to produce $\sim$50 ps, 15 μJ pulses at a 1 kHz repetition rate. Single dye laser pulses are attenuated and then split into three beams of approximately equal energy ($\sim$100 nJ). Two beams are crossed at an epitaxial interface between a c axis oriented 190 nm film of optically absorbing YBCO and an optically transparent MgO(100) or $SrTiO_3$(100) substrate as shown in Fig. 1. The c axis of the YBCO film is parallel to the x dimension and the a–b plane of the film

 0021-8979/93/020850-08$06.00

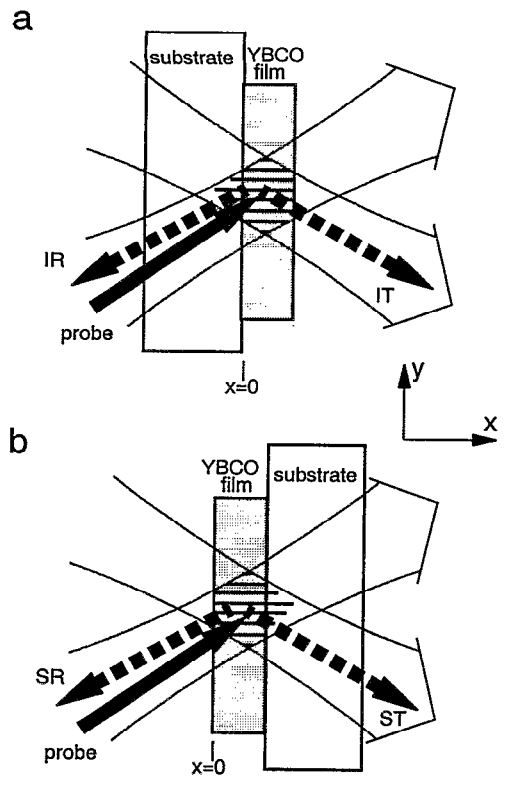

FIG. 1. Cross section of transient grating interfacial geometry for interface incident and free surface incident [parts (a) and (b), respectively] grating excitation beams denoted as outlined arrows. The probe beam and diffracted beams are denoted as a solid arrow and dashed arrows respectively in each part. IR, IT, ST, and SR refer to interface reflected, interface transmitted, surface transmitted, and surface reflected geometries of diffraction, respectively.

corresponds to the y–z plane in Fig. 1. Both MgO(100) and $SrTiO_3$(100) substrates are used. The optical density of the films is 0.9 at the experimental wavelength. A detailed description of the sample characteristics and preparation techniques are provided in the literature.[11,12]

Experiments are performed at room temperature under 10^{-6} Torr vacuum. The grating excitation beams, denoted as hollow arrows in Fig. 1, are incident from either the substrate or YBCO film side of the interface as shown in parts (a) and (b) of Fig. 1, respectively. The beams are focused to a 200 μm diam spot size and crossed at an angle 2θ in the substrate. Due to refraction the beams then cross at an angle $2\theta'$ inside the YBCO film. This produces a sinusoidal interference pattern in the YBCO and generates a grating with a wave vector parallel to the interface. Two grating fringe spacings of 0.80 and 4.25 μm were used by changing the angle between the two excitation beams. Absorption of the light produces excited electrons which rapidly thermalize[13] in several picoseconds increasing the phonon bath temperature and producing a holographic heat pattern in the film. The generation of the thermal grating (or dielectric constant modulation) leads to a density grating caused by thermal expansion of the YBCO film and by excitation of acoustic waveguide modes.[2,14,15] The grating is probed by the third pulse, that is incident at the Bragg angle from the same side of the sample as the excitation beams. The probe is temporally delayed and diffracted from the transient holographic grating in both transmitted and reflected geometries to monitor the decay of the grating as depicted by dashed lines in Fig. 1. The diffracted signal is detected with a photomultiplier tube, gated integrator, and computer.

III. NUMERICAL MODEL

The transient grating diffraction efficiency η has been recently derived for interfacial diffraction from gratings that extend on both sides of an interface.[10] The diffraction efficiency in reflection is

$$\eta^R \propto \left| \frac{\omega^2}{c^2 k_{1x}} \int_{-\infty}^{0} [2A_R + (A_R)^2 e^{-2ik_{1x}x} + e^{+2ik_{1x}x}] \Delta\epsilon(x)\,dx + \frac{\omega^2 A_T A_T'}{c^2 k_{2x}} \int_{0}^{+\infty} e^{+2ik_{2x}x} \Delta\epsilon(x)\,dx \right|^2, \tag{1}$$

and in transmission is

$$\eta^T \propto \left| \frac{\omega^2}{c^2 k_{1x}} \int_{-\infty}^{0} (1 + A_R e^{-2ik_{1x}x}) \Delta\epsilon(x)\,dx + \frac{\omega^2}{c^2 k_{2x}} \int_{0}^{+\infty} (1 - A_R e^{+2ik_{2x}x}) \Delta\epsilon(x)\,dx \right|^2, \tag{2}$$

where $\Delta\epsilon(x)$ is the grating peak to null dielectric constant modulation. Here A_R and A_T are the Fresnel reflection and transmission coefficients[16] for propagation of the undiffracted probe field from negative x to positive x across the interface, and A_T' is the Fresnel transmission coefficient for propagation in the opposite direction. The probe wave vector magnitude in vacuum is defined as $|\omega/c|$ where ω is the probe frequency and c is the speed of light in vacuum. The x component of the probe wave vector inside the substrate and film are denoted k_{1x} and k_{2x}, respectively, for excitation incident from the substrate side of the sample [Fig. 1(a)]. For the opposite or film incident excitation geometry, the wave vectors in Eqs. (1) and (2) are transposed, i.e., k_{1x} replaces k_{2x} and k_{2x} becomes k_{1x} [Fig. 1(b)]. The unperturbed dielectric constants used in the calculations are obtained from a Kramers–Kronig analysis of the reflection and transmission coefficients from the film and substrate. For the YBCO-$SrTiO_3$ sample the index of refraction is determined to be 1.5 for $SrTiO_3$ and $1.7 + i0.49$ for the YBCO. For the YBCO-MgO sample the index of refraction is determined to be 1.5 for MgO and $1.7 + i0.45$ for the YBCO. The grating amplitude, $\Delta\epsilon(x)$, is proportional to the time-dependent grating peak to null temperature difference, $\Delta T(x,t)$,

$$\Delta\epsilon(x,t) \propto \Delta T(x,t), \tag{3}$$

where the proportionality constant, which contains the complex index of refraction and the elasto-optic constant, has been derived previously.[5,17]

The grating temperature difference is obtained by solving the diffusion equation

$$\mathbf{D}\nabla^2\mathbf{T}=\frac{\partial \mathbf{T}}{\partial t}. \tag{4}$$

The diffusion equation is solved numerically using the Crank–Nickolson method[18] with the appropriate boundary and initial conditions. The vacuum surface of the 190-nm-thick YBCO film and the vacuum surface of the substrate are assumed to have reflecting boundary conditions, i.e., $dT/dx=0$. The substrates are modeled to be 3 μm wide. This width is large enough to give a negligible temperature rise at the free substrate/vacuum surface. For the substrate interface incident excitation geometry, an initial condition of

$$\mathbf{T}(x,y,z,t=0)=(T_0/2)e^{-\Omega x}[1+\cos(\beta y)] \tag{5}$$

is assumed inside the film, and

$$\mathbf{T}(x,y,z,t=0)=0 \tag{6}$$

is assumed in the substrate. Here the grating wave-vector magnitude is defined as

$$\beta=\frac{4\pi \sin(\theta)}{\lambda}, \tag{7}$$

where θ is the half angle between the two excitation beams in vacuum, and $T_0(\approx 1$–10 K) is the initial temperature jump at the incident interface. The exponential term in Eq. (5) accounts for Beer's law absorption of the excitation beams. Literature values used for the thermal diffusivity $\mathbf{D}$ are 0.05 cm^2/s for $SrTiO_3$ (Refs. 19 and 20) and 0.2 cm^2/s for MgO.[21] The solution for the dielectric constant modulation amplitude is then substituted into Eqs. (1) and (2) for the diffraction efficiency in the reflected and transmitted geometries of diffraction, respectively. The diffraction efficiency is obtained by numerical integration of Eqs. (1) and (2) over the film–substrate width.

If the grating fringe spacing is small ($\lesssim 1$ μm), then the signal decay is dominated by diffusion of heat between the grating fringes along the grating wave vector (parallel to the y axis). This gives a decay that has a dominant single exponential decay component. From the exponential decay constant, the thermal diffusivity in the plane of the film can be extracted from the relation[5]

$$\eta \propto \exp(-2D_{a-b}\beta^2 t). \tag{8}$$

Here D_{a-b} is the thermal diffusivity constant in the a–b plane of the film (y–z plane in Fig. 1).

For very large excitation spot size ($\gtrsim 1$ μm), the three-dimensional solution to the diffusion equation has a negligible effect on the transient grating signal decay from the diffusion of heat across the laser spot size.[5] For the moderately large fringe spacing used in part of this work (4.25 μm), diffusion between the grating fringes has a weak ($\sim 10\%$) effect on the transient grating signal decay rate. Rather, the signal decay is dominated by diffusion into the substrate, but diffusion between the grating fringes is also included for accuracy.

At room temperature, the acoustic mismatch model predicts a boundary resistance that is $\sim$10–100 times smaller than has been measured experimentally between $YBa_2Cu_3O_{7-x}$ (YBCO) films and MgO.[2,3,5] This discrepancy may result because the phonons do not approach the interface as coherent waves as this model assumes.[3,22,23] This incoherence is due to the short phonon mean wavelength (<10 Å) in YBCO at ~ 300 K. Consequently, the propagation of heat across the interface is modeled as perfectly diffusive in this article, i.e., there are no ballistic phonons which coherently reflect off the interface.[22] If the interface has ideal thermal contact, then any phonon that diffuses to the interface has a 50% probability of propagating either across the interface or back into the material. For an interface that has a significant thermal barrier, this symmetry is broken and the resulting probabilities are unequal. The probabilities used to model the data are linearly related to a unitless thermal barrier parameter f in the following manner. For $f=0$, the phonons have a 0% probability of diffusing through the interface corresponding to an infinite thermal boundary resistance. For a material with perfect thermal contact, $f=1$ corresponds to the 50% reflecting and 50% transmitting case described above. This can be related to the commonly used units for the thermal boundary barrier resistance R_{bd} through the relation

$$R_{bd}=\frac{w}{C_p\rho D_c f}=\frac{w}{\kappa f}, \tag{9}$$

where C_p, ρ, w, D_c, and κ are the heat capacity, density, interfacial layer width, c axis thermal diffusivity, and thermal conductivity in YBCO, respectively. An interfacial layer that is 10 Å thick is assumed since there appears to be no disorder on a distance scale larger than a unit cell for YBCO in epitaxial contact with its substrate.[24] The heat capacities of the YBCO film, 0.8 J g^{-1} K^{-1} (Ref. 25), and substrates, 0.9 J g^{-1} K^{-1} for MgO and 0.5 J g^{-1} K^{-1} for $SrTiO_3$ (Ref. 20), are incorporated into the solution of the diffusion equation to ensure conservation of energy for thermal transport across the interface.[22]

IV. RESULTS AND DISCUSSION

The anisotropic diffusion constants and the boundary resistance can be extracted by analyzing various transient grating excitation and detection geometries that emphasize different features of the thermal diffusivity process in the film and substrate. Figure 1 defines the four grating diffraction geometries used in the experiments to obtain information about the thermal flow in YBCO and through the YBCO/substrate interface.

When the grating excitation beams are incident on the free (vacuum) YBCO surface as depicted in Fig. 1(b), the deposition of heat is localized near the YBCO surface. For the surface-reflected geometry (SR), the experiment preferentially probes a region near the free surface. This leads to a situation that is ideally suited for measuring the diffusion constant along the surface normal in the YBCO film. Due to the localization of both the grating generation and signal detection near the free surface, the measurement is virtually unaffected ($\sim 1\%$ perturbation) by the thermal barrier resistance at the film–substrate interface.

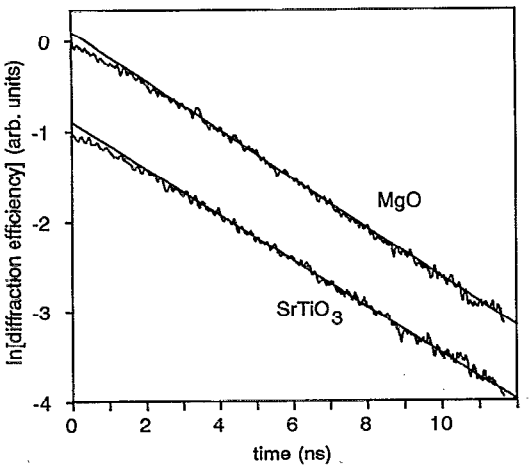

FIG. 2. Transient grating thermal signals, corrected for thermal flow across the interface, at small fringe spacing (0.80 μm) from 190 nm thick $YBa_2Cu_3O_{7-x}$ films on bulk MgO and $SrTiO_3$ substrates in parts (a) and (b), respectively. The slopes are proportional to the thermal diffusivity constants in the plane of the film.

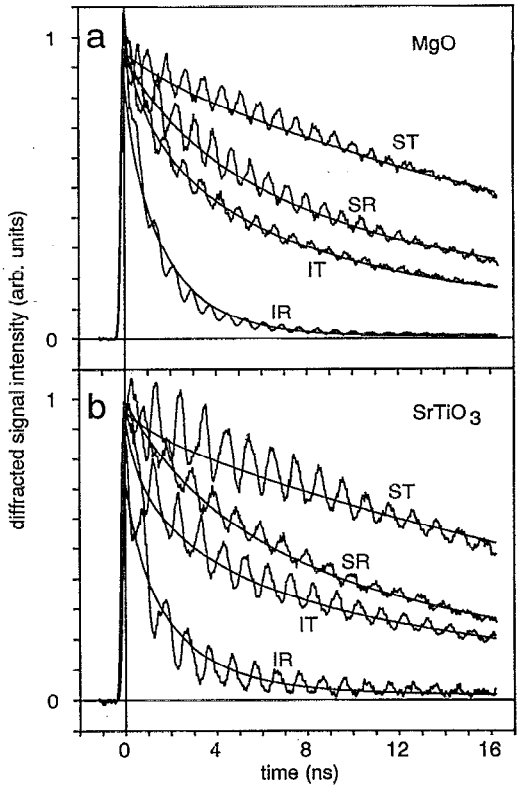

FIG. 3. Transient grating thermal signals and numerical fits at large fringe spacing (4.25 μm) from 190 nm thick $YBa_2Cu_3O_{7-x}$ films on bulk MgO and $SrTiO_3$ substrates in parts (a) and (b), respectively. Curves IR, IT, ST, and SR correspond to the diffraction geometries given in Fig. 1.

When the grating excitation beams are incident on the film/substrate interface as is depicted in Fig. 1(a), the deposition of heat is initially localized near the interface inside the film. The heat then diffuses into the bulk of the film and across the interface into the substrate. If the grating is detected in an interface-reflected or interface-transmitted geometry (IR and IT), then the experimental signal decays will be substantially affected by the magnitude of the thermal boundary resistance at the film/substrate interface.

The diffusion constants in the plane of the YBCO sample (a–b plane) can be determined from the IT geometry of diffraction with a small grating fringe spacing (0.80 μm).[5] The signal decay is dominated by heat flow from the grating peaks into the grating nulls along the grating wave vector (y axis). Flow perpendicular to the plane (along the x axis), however, weakly effects the signal due to thermal flow from the film into the substrate. To correct for the perturbative effect of thermal flow into the substrate, the data at small fringe spacing (0.80 μm) is divided by the thermal component of a data set at large fringe spacing (4.25 μm). Since the thermal flow into the MgO substrate is independent of the fringe spacing, this causes the effects of substrate thermal flow to be eliminated leaving a predominantly single exponential decay which is only related to thermal diffusivity in the plane of the film.

Figure 2 shows a logarithmic plot of the corrected transient grating data for the MgO and $SrTiO_3$ substrate samples in parts (a) and (b), respectively, with a linear regression fit through the data. The slope is proportional to the a–b plane YBCO diffusion constants which are equal to 0.023 ± 0.001 cm^2/s for the MgO substrate sample and 0.022 ± 0.001 cm^2/s for the $SrTiO_3$ substrate sample. A small deviation from the fit at short delay time (< 1 ns) in Fig. 2 is the result of an artifact in the division process from the acoustic waves in the large fringe spacing data. The diffusion constants measured here are within the error bars of those previously reported in the literature.[2,5] This indicates that the YBCO films on the MgO and $SrTiO_3$ substrates have similar crystal defect structure in the YBCO a–b plane far from the interface.

Heat flow rates across the film in the c direction (x direction) and across the interface into the substrate can be extracted by considering all four of the grating geometries illustrated in Fig. 1. By using a large fringe spacing, the data used for determining the c axis diffusion constant and barrier parameters are virtually independent of thermal flow in the plane of the film. At a relatively large fringe spacing of 4.25 μm, the signal decays about 10% due to the thermal diffusivity in the a–b plane of the sample on the 16 ns time scale of the experiment. This contribution is contained in the analysis by including the a–b plane diffusion constants obtained from the small fringe spacing experiments described above in the numerical fits to the large fringe spacing data.

Figure 3 displays the results of the transient grating experiments taken at large fringe spacing for the four diffraction geometries defined in Fig. 1. Substantially different temporal decays are observed for the different diffraction geometries. Parts (a) and (b) correspond to data taken on MgO and $SrTiO_3$ substrate samples, respectively. The smooth solid curves through the data are the results of the numerical calculations described in the previous section. The thermal diffusivities and thermal boundary resistance,

obtained by fitting the experimental data sets as described below for each substrate, are held constant between the four different diffraction geometries.

Curve SR (surface reflected) in Fig. 3 corresponds to grating excitation from the free YBCO surface and detection in the reflected diffraction geometry. The probe beam samples the closest 30 nm of the sample to the free surface preferentially. The heat is localized near the free surface immediately after the initial deposition due to the strong optical absorption of the grating excitation beams. The signal decays as heat diffuses away from the free surface region. The signal geometry is virtually unaffected by the thermal boundary resistance at the interface, making it the ideal candidate to independently determine the thermal flow rate inside the film.

The thermal (nonoscillatory) signal decays of the two SR curves in Fig. 3 have an experimentally indistinguishable temporal decay rate. The numerical fits to the SR geometry shown in Fig. 3 give a diffusion constant of 0.0026 ± 0.0002 cm^2/s for both the MgO and $SrTiO_3$ substrate samples. This is in reasonable agreement with the results previously obtained (0.0029 cm^2/s) using the transient grating method on similar oriented thin films with MgO substrates.[5] Hence, the growth of YBCO on either MgO or $SrTiO_3$ substrates does not appear to effect the thermal diffusivity either in or out of the plane of the film far from the interface. The remaining three diffraction geometries (IR, IT, and ST in Fig. 1) can now be analyzed to extract the thermal boundary resistance.

The fastest decaying signals in Fig. 3 are the IR (interface-reflected) curves. The signal decay is primarily due to heat flow through the film–substrate boundary and to the diffusion of heat away from the interfacial region into the bulk of the film. These relatively fast decay components can be attributed to three interfacial terms in Eq. (1) that describe the reflected diffraction efficiency. The three components are from the second and third terms in the brackets in the first integral and the entire second integral in Eq. (1). Each of these terms has an exponential function in the integrand that localizes the signal generation near the incident interface due to both optical absorption and interference. The remaining term in Eq. (1) is a bulk (equally weighted throughout the substrate) contribution to the signal from the substrate ($x<0$). There is an additional slowly decaying component to the signal that is relatively small in amplitude. This component arises from all the terms in Eq. (1). At long time (~ 10 ns) the offset of the IR decay primarily reflects the temperature rise in the substrate near the interfacial boundary.

In previous work the MgO was assumed to be a perfect heat sink.[5] However, because $SrTiO_3$ has a five times smaller thermal conductivity than MgO, the finite thermal flow in $SrTiO_3$ must be considered for an accurate description of the thermal distribution. The finite thermal conduction in MgO is also included for completeness, though including the finite thermal conductivity of MgO leads only to a small ($\sim 10\%$) perturbation in the measured thermal boundary resistance. For the $SrTiO_3$ substrate, where the thermal conductivity is ~ 10 times larger than along the c-axis direction in YBCO, the temperature builds up to about 20% of that in the film ~ 1 ns after the initial excitation. In contrast, the MgO substrate, where the thermal conductivity is ~ 50 times larger than in YBCO, has a temperature rise of about 5% of that in the film ~ 1 ns after the initial excitation. Since the grating diffraction efficiency is proportional to the square of the peak grating temperature change, the $SrTiO_3$ substrate sample would be expected to give a much stronger signal than the MgO substrate sample at long time. This is what the IR curves in Fig. 3 show. The amplitude of the longest decay component for the IR geometry has a marked offset for $SrTiO_3$, while for MgO there is virtually no offset. Consequently, this offset provides a measure of the substrate temperature or the efficiency of the substrate as a heat sink. In addition, since this signal is produced and detected near the interface, the short time decay (~ 2 ns) in the IR geometry is very sensitive to the magnitude of the boundary resistance.

The remaining two transmitted diffraction geometries (IT and ST) in Figs. 1 and 3 provide a mixture of signals from the bulk of the film and substrate and from the interfacial region. Consequently, they are sensitive to the redistribution of heat in both the substrate and film. All four geometries provide an over determined system that acts as a check on the particular assumptions made in modeling the system.

Three of the diffraction geometries (ST, IT, and IR) are substantially effected by the boundary resistance. The thermal barrier parameter f, defined just prior to Eq. (9), takes on a value of 0.08 ± 0.01 for the MgO substrate sample. This is about 4 times larger than in previous studies utilizing the transient grating technique on similar YBCO-MgO samples.[2,5] The samples utilized here were produced using the same basic techniques[11,12] as the samples used in previous transient grating studies,[2,5] however, they were made in a different apparatus at another location. This demonstrates that significant variation can occur in the boundary resistance as a result of sample preparation.

While the parameter f is model independent, the model for the boundary barrier resistance between YBCO and MgO is sensitive to the barrier width assumed [see Eq. (9)]. The maximum barrier width that gives good quality fits to all four diffraction geometries defined in Fig. 1 is 10 Å. This is the value that is used for the fits shown in Fig. 3. When an order of magnitude larger barrier width (100 Å) is used, the numerical calculations described in Sec. III give a significantly less precise fit to at least one of the four experimental diffraction geometries shown in Fig. 3. It is possible to fit two or three of the geometries reasonably well, but no single pair of boundary resistance and thermal diffusivity constants can be found that fit all four geometries. When the barrier width is reduced to 1 Å, the quality of the fits remains unchanged although the barrier resistance is decreased by a factor of 10 [see Eq. (9)]. An upper limit of about 10 Å can therefore be placed on the effective barrier width in contrast to the 100 Å barrier width assumed in other work.[1,4] This illustrates the potential power that the transient grating technique can have by incorporating multiple diffraction geometries into the experiment.

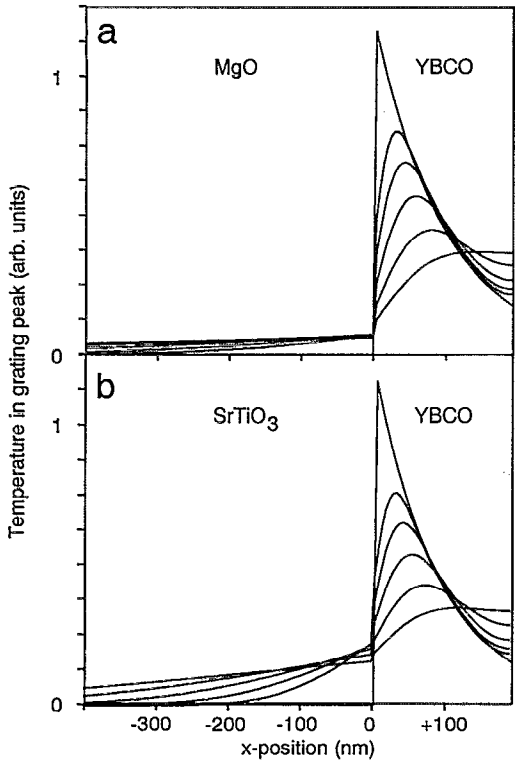

FIG. 4. Thermal distributions in the grating peaks used for the calculations of the IT and IR fits in Fig. 3, both inside the $YBa_2Cu_3O_{7-x}$ (YBCO) films for $x>0$, and in the MgO [part (a)] and $SrTiO_3$ [part (b)] substrates for $x<0$. The six curves in each part represent the temperature profiles 0, 1, 2, 4, 8, and 16 ns, in decreasing height, respectively, after the initial grating excitation.

TABLE I. Summary of thermal boundary resistance measurements performed between $YBa_2Cu_3O_{7-x}$ thin films and a variety of substrates taken from the literature and as reported in this work. All samples are thin films (0.01–1 μm) in epitaxial contact with the substrate unless otherwise noted.

Thermal boundary resistance ($cm^2\,K\,W^{-1}$)	Remarks	Reference
1.1×10^{-3}	110 K on $LaAlO_3$ substrate	3
1.3×10^{-3}	100 K on sapphire substrate with 100 Å $SrTiO_3$/100 Å MgO overlayers	3
1.2×10^{-3}	100 K on sapphire substrate with 200 Å $LaAlO_3$ overlayer	3
0.9×10^{-3}	100 K on sapphire substrate with 500 Å $CaTiO_3$ overlayer	3
20	230 K, nonepitaxial ruby substrate clamped to bulk superconductor sample	6
3×10^{-3}	~90 K on $LaAlO_3$ substrate; assumes 100 Å barrier width	4
1×10^{-3}	~80 K on $LaAlO_3$ substrate; assumes 100 Å barrier width	1
5×10^{-4}	300 K on MgO substrate; assumes 10 Å barrier width	2
5×10^{-4}	Constant from 90–300 K on MgO substrate Resistance is ~2 times smaller at 20 K; assumes 10 Å barrier width	5
1×10^{-4}	300 K on MgO substrate; assumes 10 Å barrier width	this work
Maximum of $\sim1\times10^{-4}$	300 K on $SrTiO_3$ substrate; assumes 10 Å barrier width	this work

If only one of the geometries that is sensitive to the boundary resistance is utilized, for example, the IT geometry, it would not be possible to obtain information about the effective barrier width.

The $SrTiO_3$ substrate sample does not have a clearly defined thermal barrier parameter. In addition to the boundary resistance, the decays are measurably effected by the finite thermal conductivity in the substrate. The fits shown in Fig. 3 are calculated with $f=0.16$. However, any value between 0.10 and 1.0 gives equally good fits to the four data sets in Fig. 3(b). This arises from the fact that the finite thermal conductivity in the substrate limits the thermal flow out of the film as much as, if not more than, the barrier itself.[22] This can be seen by inspecting the thermal spatial distributions inside the samples shown in Fig. 4. These distributions are the intermediate results in calculating the final diffraction efficiency fits in Fig. 3. Figure 4 presents the thermal distributions for the interfacial excitation geometry [Fig. 1(a)] that are calculated for the IR and IT transient grating data in Fig. 3. The interface between the film and substrate in Fig. 4 is located at $x=0$ and the free film surface is located at $x=190$ nm. Only the nearest 400 nm to the interface are shown for the substrate thermal profile, although the numerical calculation grid extends 7.5 times further out.

The thermal profiles inside the YBCO films (positive side of the x axis) are very similar for both the MgO and $SrTiO_3$ substrates shown in parts (a) and (b) of Fig. 4, respectively. However, the thermal profiles on the substrate side of the interface are substantially different. For the MgO substrate in Fig. 4(a), the temperature profile has a relatively small maximum temperature in the substrate and is spatially uniform on a distance scale of 100 nm. In contrast, the $SrTiO_3$ substrate in Fig. 4(b) has a temperature rise about four times higher near the interface with a substantial spatial gradient due to the relatively slow thermal diffusivity in the substrate. After about 4 ns, the temperature discontinuity, or jump, across the interface is almost zero for the $SrTiO_3$ substrate, i.e., $T_{substrate}\cong T_{film}$ at $x=0$. For MgO, however, even after 16 ns the temperature jump across the film–substrate interface is approximately equal to the temperature in the substrate at the interface. This illustrates the important role that a finite thermal conductivity in the substrate has on thermal flow across an interface.

Literature values for the thermal barrier resistance are summarized in Table I and compared to the measurements performed in this paper. The results vary by about one order of magnitude for the epitaxial films depending on preparation techniques and measurement methods. Some

of the measurements in the literature presumed a 100 Å barrier width.[1,4] The boundary resistance would have been reduced an order of magnitude for these measurements if a 10 Å barrier width had been assumed as in this paper. This illustrates the importance of determining an accurate barrier width.

For either barrier width (10 or 100 Å), all of the thermal boundary resistances are ~10–100 times larger than predicted by the acoustic mismatch model.[22] A T^{-3} temperature dependence for the thermal boundary resistance would be indicative of the acoustic mismatch model for ballistic phonons. However, there is no evidence in the literature for such a steep temperature dependence over the range 10–300 K for YBCO epitaxial films.[3–5] The thermal boundary resistance actually changes much less than one order of magnitude between 10 and 300 K. The barrier must therefore be diffusive in nature for temperatures significantly greater than 10 K. The physical origin of the large boundary resistance may arise from a nonuniform interfacial thermal conductivity[26] or from the nature of the phonon mode structure near the interface due to the complex crystal configuration of YBCO.[27,28] For rapid thermal energy transport across an interface, there must be a good overlap of the phonon density of states and mode displacements in the two materials.[22,29] The elementary substrate crystal structures (MgO, $LaAlO_3$, $CaTiO_3$, and $SrTiO_3$) that have been utilized to date[1,3–5] all have relatively simple phonon structures, which may explain the similar thermal boundary resistances that have been observed for YBCO epitaxial films on different crystalline substrates. MgO would be expected to have the fewest low frequency optical phonon modes since it has the least complicated crystal structure. This implies that YBCO-MgO interfaces would have one of the largest thermal boundary resistances for epitaxial contact based on a density of states argument.

V. CONCLUDING REMARKS

The thermal transient grating technique has been demonstrated to be an effective technique for determining the thermal transport rates in thin films and the nature of microscopic thermal contact between two materials. The technique has the advantage of being an all optical nondestructive method, since no mechanical contact is made with the sample. By using multiple grating excitation and detection geometries, detailed information about the spatial distribution is obtained that would not otherwise be available from a single excitation or probe geometry. For example, it was possible to determine the maximum thickness of the thermal interfacial barrier.

The anisotropic bulk thermal diffusivity constants in 190 nm thin films of $YBa_2Cu_3O_{7-x}$ (YBCO) have been measured. The diffusivity measurements reported here are in good agreement with previously measured values. Boundary resistance measurements have been performed on YBCO thin films in epitaxial contact with MgO and $SrTiO_3$ substrates. A maximum barrier width of ~10 Å has been inferred from the simultaneous measurement of four different transient grating diffraction geometries. The four geometries probe different regions in the sample preferentially, providing information about the spatial distribution of the thermal flow rates. The thermal flow from YBCO to a $SrTiO_3$ substrate is shown to be limited by the finite thermal conductivity inside the bulk substrate. Consequently, only an upper limit can be placed on the boundary resistance for the YBCO-$SrTiO_3$ interface.

ACKNOWLEDGMENTS

We would like to thank T. H. Geballe for many useful discussions throughout the course of this work. This work was supported by the National Science Foundation, Division of Materials Research (Grant No. DMR90-22675) and by the Office of Naval Research, Physics Division (Grant No. N00014-89-J1119). I.M.F. would like to acknowledge support by the Medical Free Electron Laser Program, Office of Naval Research (Grant No. N00014-91-C0170).

[1] G. L. Carr, M. Quijada, D. B. Tanner, C. J. Hirschumgl, G. P. Williams, S. Etemad, B. Dutta, F. DeRosa, A. Inam, T. Venkatesan, and X. Xi, Appl. Phys. Lett. **57**, 2725 (1990).
[2] C. D. Marshall, I. M. Fishman, and M. D. Fayer, Phys. Rev. B **43**, 2696 (1991).
[3] M. Nahum, S. Verghese, P. L. Richards, and K. Char, Appl. Phys. Lett. **59**, 2034 (1991).
[4] C. G. Levey, S. Etemad, and A. Inam, Appl. Phys. Lett. **60**, 126 (1992).
[5] C. D. Marshall, I. M. Fishman, R. C. Dorfman, C. B. Eom, and M. D. Fayer, Phys. Rev. B **45**, 10009 (1992).
[6] B. M. Terzijska, R. Wawryk, D. A. Dimitrov, C. Marucha, and J. Rafalowicz, Cryogenics **32**, 53 (1992).
[7] D. H. Martin and D. Bloor, Cryogenics **1**, 1 (1961).
[8] P. L. Richards, J. Clarke, R. Leoni, P. Lerch, S. Verghese, M. R. Beasley, T. H. Geballe, R. H. Hammond, P. Rosenthal, and S. R. Spielman, Appl. Phys. Lett. **54**, 283 (1989).
[9] I. M. Fishman, C. D. Marshall, J. S. Meth, and M. D. Fayer, J. Opt. Soc. Am. B **8**, 1880 (1991).
[10] I. M. Fishman, C. D. Marshall, A. Tokmakoff, and M. D. Fayer (unpublished).
[11] C. B. Eom, J. Z. Sun, S. K. Sun, S. K. Streiffer, A. F. Marshall, K. Yamamoto, B. M. Lairson, S. M. Anlage, J. C. Bravman, T. H. Geballe, S. S. Laderman, and N. R. C. Paber, Physica C **171**, 351 (1990).
[12] C. B. Eom, J. Z. Sun, K. Yamamoto, A. F. Marshall, K. E. Luther, T. H. Geballe, and S. S. Laderman, Appl. Phys. Lett. **55**, 595 (1989).
[13] S. D. Borson, A. Kazeroonian, J. S. Moodera, D. W. Face, T. K. Cheng, E. P. Ippen, M. S. Dresselhaus, and G. Dresselhaus, Phys. Rev. Lett. **64**, 2172 (1990).
[14] B. A. Auld, *Acoustic Fields and Waves in Solids* (Wiley, New York, 1973), Vol. II, Chap. 10.
[15] J. S. Meth, C. D. Marshall, and M. D. Fayer, J. Appl. Phys. **67**, 3362 (1990).
[16] M. Born and E. Wolf, *Principles of Optics* (Pergamon, Oxford, 1970).
[17] K. A. Nelson, R. Casalegno, R. J. D. Miller, and M. D. Fayer, J. Chem. Phys. **77**, 1144 (1982).
[18] W. H. Press, B. P. Flannery, S. A. Teokolsky, and W. T. Vetterling, *Numerical Recipes in C* (Cambridge University Press, Cambridge, 1988).
[19] Y. S. Touloukian, R. W. Powell, C. Y. Ho, and P. G. Klemens, *Thermal Conductivity: Nonmetallic Solids. Thermophysical Properties of Matter* (Plenum, New York, 1970).
[20] Y. S. Touloukian and E. H. Buyco, *Thermophysical Properties of Matter* (Plenum, New York, 1970).
[21] Y. S. Touloukian, R. W. Powell, C. Y. Ho, and M. C. Nicolaou, *Thermal Diffusivity: Thermophysical Properties of Matter* (Plenum, New York, 1973).
[22] K. E. Gray, *Nonequilibrium Superconductivity, Phonons, and Kapitza Boundaries* (Plenum, New York, 1981).
[23] W. A. Little, Can. J. Phys. **37**, 334 (1959).
[24] S. K. Streiffer, B. M. Lairson, C. B. Eom, B. M. Clemens, J. C. Brav-

man, and T. H. Geballe, Phys. Rev. B **43**, 13007 (1991).
[25] S. B. Peralta, Z. H. Chen, and A. Mandelis, Appl. Phys. A **52**, 289 (1991).
[26] I. M. Fishman, Bull. Am. Phys. Soc. **37**, 246 (1992).
[27] J. D. Jorgensen, Physics Today **45**, 34 (1991).
[28] V. G. Baryakhtar, A. A. Vasilkevich, P. G. Ivanitsky, V. T. Krotenko, A. N. Maistrenko, A. E. Morozovsky, V. M. Pan, M. V. Pasechnik, and V. I. Slisenko, Physica C **162–164**, 466 (1989).
[29] R. J. Stoner, H. J. Maris, T. R. Anthony, and W. F. Banholzer, Phys. Rev. Lett. **68**, 1563 (1992).